Method for Analyzing Structural Changes of Flexible Metal−Organic Frameworks Induced by Adsorbates

D. Dubbeldam,*,† R. Krishna,† and R. Q. Snurr‡

Van't Hoff Institute for Molecular Sciences, University of Amsterdam, Nieuwe Achtergracht 166, Amsterdam, The Netherlands, and Chemical and Biological Engineering Department, Northwestern University, 2145 Sheridan Road, Evanston Illinois 60208

Received: July 14, 2009; Revised Manuscript Received: September 16, 2009

Metal−organic frameworks (MOFs) have crystal structures that exhibit unusual flexibility. An extreme example is that of the "breathing MOF" MIL-53 that expands or shrinks to admit guest molecules like CO_2 and water. We present a powerful simulation tool to quickly calculate unit cell shape and size at 0 K for structures loaded with adsorbates. The method can be applied to unit cell minimization of periodic systems such as metal−organic frameworks and zeolites for vibrational analysis (IR spectra and mode analysis), force field development, and computation of elastic constants at 0 K. The expressions for first- and second-derivatives for rigid guest molecules that are missing in the literature are described in this paper. In addition, two case studies about determination of the structure of IRMOF-1 at 0 K and about the influence of water on the structure of MIL-53 showed that the simulation results correspond well with experimental results and other computational results. Our analysis scheme has significant advantages over other schemes, and the IRMOF-1 case study shows how these methods could potentially fail.

Introduction

Adsorption and diffusion inside porous solids is an important phenomenon for many practical applications, including purification of gases and liquids, decolorizing sugar, chromatography, membrane technology, and catalysis.[1,2] The field of metal−organic frameworks (MOFs) has undergone an impressive growth over the past decade. Some 4,000 frameworks are currently known to exist, and nearly 1000 new MOFs are reported each year.[3] MOFs are nanoporous, molecule-based, hybrid materials built from metal nodes and organic bridging ligands. MOFs have good stability, high void volumes, and well-defined tailorable cavities of uniform size.[1,4−10] Developing simulation models for MOFs represents a major challenge because MOFs are often flexible and can shrink and swell upon adsorption as well as change space group as a function of loading and temperature.[11−15] Many models for nanoporous materials are presently available.[16] Among these for zeolites are models of Demontis et al.,[17] Nicholas et al.,[18] Hill et al.,[19,20] and the core−shell models.[21−25] For metal−organic frameworks, the models are specific to certain groups of structures. The first models were developed for Iso-Reticular MOFs (IRMOFs) such as the models by Greathouse and Allendorf,[26,27] Dubbeldam et al.,[28] Amirjalayer et al.,[29−31] and Han and Goddard.[32] A model for the covalent organic frameworks (COFs) was developed by Amirjalayer et al.[33] For a breathing structure, MIL-53, models were developed by Salles et al.[34] and Coombes et al.[35] All of these MOF models are largely based on generic force fields like CVFF,[36] DREIDING,[37] UFF,[38] or MM3[39] with missing parameters filled in or refined using empirical fitting and/or quantum mechanical approaches.

A crucial step in model development is to compare structural properties to experiments and/or quantum mechanical computations. The latter has significant advantages because it provides a theoretical sound and consistent basis for force field development. For example, it eliminates experimental difficulties related to the quality of the crystal sample. Classical and quantum mechanical simulations can quickly and accurately be compared in detail at 0 K. A first step in this process is the minimization of the crystal structure. The quantum mechanical reference values need to be computed only once, but for the classical minimizations, we may want to minimize many times to refine the potential parameters. We therefore require a reliable, fast, and general method that guarantees accurate results. In this paper, we describe and develop such a method. Molecular mechanics minimizations are useful for comparing structures, computing binding energies, harmonic analysis, fitting force fields, initial state preparation, docking, and many other purposes. They provide information that is complementary to molecular dynamics (MD) and Monte Carlo (MC). Ensembles of structures are useful for calculating thermodynamic averages and estimating entropy, but the large number of structures makes detailed microscopic analysis more difficult. Minimized structures represent the underlying configurations about which fluctuations occur during dynamics. The potential energy surface U of a (periodic) system can be Taylor-expanded around a configuration $\mathbf{x}$ of the system

$$U(\mathbf{x}+\delta\mathbf{x}) = U(\mathbf{x}) + \mathbf{h}^T\delta\mathbf{x} + \frac{1}{2}\delta\mathbf{x}^T\mathscr{H}\delta\mathbf{x} + \ldots \quad (1)$$

where $\mathbf{h} = (\partial U)/(\partial x)$ is the gradient and $\mathscr{H} = (\partial^2 U)/(\partial x_\alpha \partial x_\beta)$ is usually referred to as the Hessian matrix. The superscript T denotes the transpose of a vector or matrix. The Supporting Information contains more information on classical molecular force fields. The real potential energy surfaces of common force

* To whom correspondence should be addressed. E-mail: D.Dubbeldam@uva.nl.
† Van't Hoff Institute for Molecular Sciences.
‡ Northwestern University.

10.1021/jp906635f CCC: $40.75
Published on Web 10/12/2009

fields are rarely harmonic, but still the expansion is usually truncated at the second order (i.e., harmonic analysis). This assumes the energy surface is at least locally quadratic and can iteratively be used to find the nearest local minimum. The steps through the energy landscape can therefore not be too large. If the potential energy surface truly was quadratic, a method like Newton−Raphson would be able to find the minimum energy configuration in a single step. At the minimum energy configuration, the first derivatives are zero, and all harmonic information on the system is therefore described by the Hessian matrix.

The following sets of algorithms are commonly employed for local energy minimization:[40] methods which only use the energy (e.g., simplex method[41,42]); methods which use the energy and first derivatives (e.g., steepest descent, conjugate gradient, and Snyman's method[43,44]); methods which use the energy, first derivatives, and approximate second derivatives (e.g., Quasi-Newton method); methods which use the energy, first derivatives, and exact second derivatives (e.g., Newton−Raphson); and methods which use the energy, first derivatives, second derivatives, and the eigenvalues and eigenvectors of the Hessian matrix (e.g., mode-following technique,[45] also known as Baker's minimization[46]). The conjugate gradient minimization is the most commonly used technique. Whereas steepest descent takes a step always based on the gradient, the conjugate gradient method starts along the steepest descent direction, continues along this direction until a minimum is reached, but then proceeds along a perpendicular (or "conjugate") direction.

The Newton−Raphson method uses not only the first derivatives but also the Hessian matrix. At the cost of more memory and computation, the algorithm becomes more reliable and has an accelerated convergence (fewer steps are needed). In addition, methods that use second derivatives lead to first derivatives that can be lowered arbitrarily close to zero. The Newton−Raphson algorithm tends to find stationary points that are of the same curvature, i.e., the same number of negative eigenvalues of the Hessian matrix as the Hessian at the starting point. The eigenmode-following technique solves this limitation by shifting some of the eigenvalues to change their sign and achieve the desired curvature. Importantly, out of the discussed methods, only the eigenmode-following technique guarantees that a true minimum is found. Other methods should employ a check afterward to determine whether the stationary point is a true minimum.

In this work, we explore the eigenmode-following technique for the minimization of unit cells of periodic structures such as zeolites, metal−organic frameworks, clays, glasses, etc. It can be applied to crystalline and non-crystalline systems as long as a description for a unit cell is available. Finite systems are also easily handled by using appropriate boundary conditions. We allow for the possibility that the guest molecules are rigid, whereas the host is flexible. As minimization variables, we chose the Cartesian coordinates of the framework atoms, center of mass positions, elements of the rotation matrices for rigid guest molecules, and the elements of the strain matrix to allow the cell to change size and shape. Cartesian coordinates can be defined for all systems, and the energy potential, gradients, and Hessians are usually calculated directly in Cartesian coordinates. Instead of Cartesian coordinates, one can also choose redundant or non-redundant internal coordinates.[47−53] The matrix of second derivatives contains second derivatives with respect to center of mass position and rotation elements but also with respect to strain. We derive expressions, not available in the published literature, for these derivatives, following the procedure of Lutsko.[54] The use of analytical derivatives is preferred as they are exact and can be calculated quickly. The resulting minimization scheme is fast, reliable, and flexible.

The remainder of this paper is organized as follows. We start by describing the system and the variables to minimize, the mode-following technique, and the expressions for first and second derivatives that are missing in the literature for common classical force fields. We discuss two case studies on MOFs focusing on the advantage of the mode-following technique and show it gives the correct solution whereas other methods fail. Throughout the paper, the Einstein summation convention is used. Greek indices denote $\{x, y, z\}$ for positions and $\{1, 2, 3\}$ for orientation. Graphics in this work were generated using VMD[55] and VTK.[56,57]

Mode-Following Minimization Technique for Rigid Molecules

In order to not only optimize the position of the particles, but also to allow the simulation cell to change shape and size, a generalized Hessian matrix can be constructed that includes variables of the cell.[53,58] It is customary to choose the six elements of the strain matrix as additional generalized coordinates.[24,25,58] In this work, we combine this approach with a recently proposed matrix formulation for rigid bodies by Chakrabarti and Wales.[59]

In crystallography, the crystal structure is defined by the unit cell edge lengths a, b, and c, angles α, β, and γ, and fractional coordinates of the atoms within the unit cell.[60] Fractional coordinates form an orthonormal dimensionless space. The transformation from fractional space to real Cartesian space can be carried out by the matrix $\mathbf{H}$

$$\mathbf{H} = \begin{pmatrix} a & b\cos(\gamma) & c\cos(\beta) \\ 0 & b\sin(\gamma) & c\zeta \\ 0 & 0 & c\sqrt{1-\cos^2\beta-\zeta^2} \end{pmatrix} \tag{2}$$

with

$$\zeta = \frac{\cos\alpha - \cos\gamma\cos\beta}{\sin\gamma} \tag{3}$$

The cell matrix $\mathbf{H}$ consists of the three column cell vectors $\mathbf{a}$, $\mathbf{b}$, and $\mathbf{c}$. The matrix $\mathbf{H}$ here conforms to the standard orientation: $\mathbf{a}$ is oriented along the x axis and $\mathbf{b}$ is confined to the xy plane. The inverse cell matrix $\mathbf{H}^{-1}$ consists of the three reciprocal lattice vectors $\mathbf{a}^*$, $\mathbf{b}^*$, and $\mathbf{c}^*$[61]

$$\mathbf{a}^* = \frac{\mathbf{b}\times\mathbf{c}}{V}, \mathbf{b}^* = \frac{\mathbf{c}\times\mathbf{a}}{V}, \mathbf{c}^* = \frac{\mathbf{a}\times\mathbf{b}}{V} \tag{4}$$

where $V = |\mathbf{a}\cdot\mathbf{b}\times\mathbf{c}|$ is the volume of the unit cell. We define the reciprocal lattice vectors $\mathbf{k}$ by $\mathbf{k} = 2\pi(k_1\mathbf{a}^* + k_2\mathbf{b}^* + k_3\mathbf{c}^*)$ with k_1, k_2, and k_3 integers not all zero. The inverse cell matrix $\mathbf{H}^{-1}$ transforms Cartesian coordinates $\mathbf{r}$ to fractional coordinates $\mathbf{s}$. With the chosen $\mathbf{H}$, the scaled box has a length of 1. Usually, the potentials of the force field are defined in real space; therefore, it is convenient to store positions in Cartesian space. Distance vectors $\mathbf{r}_{ij}$ are transformed to fractional space, periodic boundary conditions are applied in fractional space, and the distance vectors are transformed back to Cartesian space to compute distances within the simulation box

$$\begin{aligned} \mathbf{s}_{ij} &= \mathbf{H}^{-1}\mathbf{r}_{ij} \\ \mathbf{s}'_{ij} &= \mathbf{s}_{ij} - \mathrm{rint}(\mathbf{s}_{ij}) \\ \mathbf{r}'_{ij} &= \mathbf{H}\mathbf{s}'_{ij} \end{aligned} \tag{5}$$

where the "rint" function returns the rounded integer value of its argument.

In the method that we will outline, we use a single crystallographic unit cell. Each particle in the unit cell interacts with all other particles in the unit cell but also with all the images in the surrounding replica cells as shown in Figure 1. The smallest perpendicular width of the simulation cell has to be larger than twice the spherical cutoff in Cartesian space. This requirement determines the number of "replica" unit cells that needs to be constructed. As we will soon see, the bottleneck in the method is the computation of eigenvectors and values of the Hessian matrix. For example, the asymmetric unit cell of α-quartz contains 2 atoms: oxygen at fractional position (0.41360, 0.26760, 0.21410) and silicon at (0.47010, 0.00000, 0.33333). The cell is described by a = 4.913 Å, b = 4.913 Å, c = 5.4052 Å, $\alpha = \beta = 90°$, and $c = 120°$. The space group is 152, and there are 9 atoms in the full unit cell. If our force field uses a van der Waals cutoff of 12 Å, then we need to use a sufficient number of "replica" unit cells, e.g. 6 × 6 × 5, to allow for a correct computation. Importantly, the computation of the Hessian matrix is based on the 9 atoms in the unit cell [the computation of eigenvalues and vectors of a $n \times n$ matrix is expensive for large systems because it scales as (n^3)].

Strain describes the deformation of a unit cell from some reference state. The strain tensor η can be defined by[54]

$$\eta = \begin{pmatrix} \eta_1 & \frac{1}{2}\eta_2 & \frac{1}{2}\eta_3 \\ \frac{1}{2}\eta_2 & \eta_4 & \frac{1}{2}\eta_5 \\ \frac{1}{2}\eta_3 & \frac{1}{2}\eta_5 & \eta_6 \end{pmatrix} = \frac{1}{2}[(\mathbf{H}_0^{-1})^{\mathrm{T}}\cdot\mathbf{H}^{\mathrm{T}}\cdot\mathbf{H}\cdot\mathbf{H}_0^{-1} - \mathbf{I}] \tag{6}$$

where $\mathbf{H}_0$ is the reference value of $\mathbf{H}$ ($\mathbf{H}_0$ can be either stress-free or stressed), $\mathbf{H}^{\mathrm{T}}$ is the transpose of $\mathbf{H}$, and $\mathbf{I}$ is the identity matrix. The six independent strain elements give the change in positions and the cell matrix relative to the reference values, assuming the origin is at (0,0,0)

$$\mathbf{r} = \eta\mathbf{r}_0 \tag{7}$$

$$\mathbf{H} = \eta\mathbf{H}_0 \tag{8}$$

Further details on strain, stress, and pressure are given in the Supporting Information.

There are many molecular models for adsorbates that treat the molecule as rigid. Among the many examples are water,[62] benzene,[63] and CO_2.[64] There are three basic approaches to satisfying constraints: unconstrained coordinates ("internal coordinates"), explicit constraint forces, and minimizing constraint forces implicitly by the technique of Lagrange multipliers[65,66] or projection methods.[67−69] Recently, Chakrabarti and Wales introduced a method based on the first approach.[59] They introduced a matrix formulation that is robust and efficient for rigid-body geometry optimization. The six degrees of freedom for a nonlinear rigid body can be defined as the center of mass

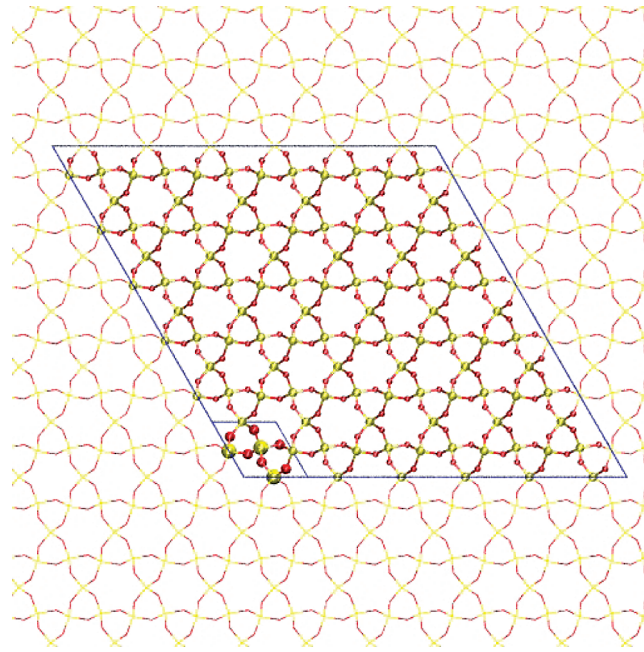

Figure 1. Single unit cell of α-quartz is shown, containing 9 atoms. We use periodic boundary conditions, and the atoms periodically repeat around the central unit cell extending to infinity. In order to compute van der Waals forces, the unit cell is explicitly surrounded by enough replica cells to obey the minimum image convention. Here, for a cutoff of 12 Å, we need to use 6 × 6 × 5 replica cells.

coordinates $\mathbf{r} = (r_1, r_2, r_3)$ and the three components of a vector $\mathbf{p} = (p_1, p_2, p_3)$, which specifies both a rotation axis through the center of mass and a magnitude of rotation $\theta = (p_1^2 + p_2^2 + p_3^2)^{1/2}$. For the rotation vector $\mathbf{p}$, the corresponding 3 × 3 rotation matrix $\mathbf{R}$ can be expressed as (Rodrigues' rotation formula)

$$\mathbf{R} = \mathbf{I} + \tilde{\mathbf{p}}\sin\theta + \tilde{\mathbf{p}}^2(1 - \cos\theta) \tag{9}$$

where $\tilde{\mathbf{p}}$ is the skew-symmetric matrix obtained from the unit vector $\hat{\mathbf{p}}$

$$\tilde{\mathbf{p}} = \frac{1}{\theta}\begin{pmatrix} 0 & -p_3 & p_2 \\ p_3 & 0 & -p_1 \\ -p_2 & p_1 & 0 \end{pmatrix} \tag{10}$$

The product of the skew-symmetric matrix $\tilde{\mathbf{p}}$ and any vector $\mathbf{v}$ returns their cross product $\tilde{\mathbf{p}}\mathbf{v} = \mathbf{p} \times \mathbf{v}$. The derivatives of the rotation matrix $(\partial^2\mathbf{R})/(\partial p_\alpha^2)$ and $(\partial^2\mathbf{R})/(\partial p_\alpha \partial p_\beta)$ are denoted by $\mathbf{R}_{\alpha\alpha}$ and $\mathbf{R}_{\alpha\beta}$ and given by Chakrabarti and Wales[59] and for convenience are also given in the Supporting Information. The advantage of this scheme is that "all the rigid-body coordinate information is stored in the space-fixed frame, and the derivatives of the rotation matrix can all be programmed in general using a fixed subroutine, which can be called to deal with site−site isotropic potentials as well as single-site or site−site anisotropic potentials".[59]

One can differentiate the energy Taylor expansion eq 1 with respect to $\delta\mathbf{x}$, set the result to zero, and solve to obtain what is known as the Newton−Raphson step[70]

$$\delta\mathbf{x} = -\mathscr{H}^{-1}\mathbf{h} \tag{11}$$

The Newton−Raphson step can also be expressed as a sum over the eigenvectors $\mathbf{e_i}$ (called local principle modes) and eigenvalues λ_i of the Hessian matrix

$$\delta\mathbf{x} = -\sum_i \frac{(\mathbf{e}_i^{\mathrm{T}}\mathbf{h})}{\lambda_i}\mathbf{e}_i \tag{12}$$

where $\mathbf{e}_i^{\mathrm{T}}\mathbf{h}$ is the component of the gradient along the eigenmode $\mathbf{e}_i$. For zero eigenvalues, the corresponding step component is set to zero. A zero eigenvalue means that for a displacement in the direction of the eigenvector the energy does not change, while a positive and negative value mean an increase and decrease in energy, respectively. Therefore, a true minimum has all positive eigenvalues. A first-order saddle point has exactly one negative eigenvalue. The Newton−Raphson steps minimize along the eigenvectors with positive eigenvalues and maximize along eigenvectors with negative eigenvalues. Therefore, when the starting configuration is of the correct curvature (the desired number of negative eigenvalues), the Newton−Raphson step is a good one to take.

In general however, the step must be modified to obtain a structure of the desired curvature.[46] A simple but very powerful modification is to use a shift parameter γ, which shifts the value of the eigenvalues[71]

$$\delta\mathbf{x} = -\sum_i \frac{\mathbf{e}_i^{\mathrm{T}}\mathbf{h}}{\lambda_i - \gamma}\mathbf{e}_i \tag{13}$$

Simons et al.[72] derived an equation to find the shift parameter

$$\gamma = -\sum_i \frac{(\mathbf{e}_i^{\mathrm{T}}\mathbf{h})^2}{\gamma - \lambda_i} \tag{14}$$

which can be solved by iteration. Note that besides minimization, the method can also be used to find saddle points.[46]

Taking a big step leads to an increased likelihood of moving out of the region where the Hessian was valid. Therefore, it makes sense to set a maximum tolerance on the size of any calculated $\delta\mathbf{x}$ and scale down $\delta\mathbf{x}$ accordingly if this maximum is exceeded.[72] The mode-following technique is also applicable to minimizations of large quantum mechanical systems. Here, the analytical evaluation of the Hessian might be computational and memory demanding, but efficient parallel distributed data algorithms have been developed.[73]

Mode-following techniques are available in many codes, e.g., GULP.[24,25] Here, we extend the method to include rigid adsorbates using the matrix-formulation of Chakrabarti and Wales.[59] In the next section, we provide the necessary expressions for first and second derivatives.

Analytical Expressions for Strain Derivatives and Generalized Hessian

If the coordinates of two rigid bodies are denoted I and J and the sites within each rigid body by i and j, then for site−site isotropic potentials the total energy is

$$U = \sum_{I<J}\sum_{i\in I}\sum_{j\in J} f_{ij}(r_{ij}) \tag{15}$$

where $r_{ij} = |\mathbf{r}_i^I - \mathbf{r}_j^J|$ is the distance between the position $\mathbf{r}_i^I$ of site i of rigid unit I and the position $\mathbf{r}_j^J$ of site j of rigid unit J, and f_{ij} is the pair potential between these sites. In general, the superscript I denotes properties related to rigid unit I. Note that in this work, van der Waals cutoffs are applied between sites (in contrast to, for example, a molecular cutoff where all sites of molecule I interact with molecule J when the center of mass distance falls within the molecular cutoff). If ξ represents one of the six generalized coordinates of rigid body I, then the first derivative of the potential energy is

$$\frac{\partial U}{\partial \xi} = \sum_{J\neq I}\sum_{i\in I}\sum_{j\in J} f'_{ij}(r_{ij})\frac{\partial r_{ij}}{\partial \xi} \tag{16}$$

The potential derivative is given by

$$f'_{ij} = \frac{\mathrm{d}f_{ij}(r_{ij})}{\mathrm{d}r_{ij}} \tag{17}$$

and we define f_1 and f_2 as[59]

$$f_1(r_{ij}) = \frac{f'_{ij}(r_{ij})}{r_{ij}} \tag{18}$$

$$f_2(r_{ij}) = \frac{f'_1(r_{ij})}{r_{ij}} \tag{19}$$

The first derivatives are

$$\frac{\partial r_{ij}}{\partial \mathbf{r}^I} = \hat{\mathbf{r}}_{ij} \tag{20}$$

$$\frac{\partial r_{ij}}{\partial p_\alpha^I} = \hat{\mathbf{r}}_{ij}\cdot\frac{\partial \mathbf{r}_{ij}}{\partial p_\alpha^I} = \hat{\mathbf{r}}_{ij}\cdot(\mathbf{R}_\alpha^I\mathbf{r}_i^0) \tag{21}$$

where

$$\mathbf{r}_{ij} = (\mathbf{r}^I + \mathbf{R}^I\mathbf{r}_i^0) - (\mathbf{r}^J + \mathbf{R}^J\mathbf{r}_j^0) \tag{22}$$

is used. Here, $\mathbf{r}^I$ is the position of the center of mass of rigid unit I, $\mathbf{R}^I$ is the rotation matrix of rigid unit I, and $\mathbf{r}_i^0$ is the position of site i in the molecular body-fixed frame.

The strain derivative for atoms is

$$\frac{\partial U}{\partial \eta_{\alpha\beta}} = \sum_{j\neq i} f_1 r_{ij,\alpha} r_{ij,\beta} \tag{23}$$

and the strain derivative for rigid units reads

$$\frac{\partial U}{\partial \eta_{\alpha\beta}} = \sum_{J\neq I}\sum_{i\in I}\sum_{j\in J}\left[f_1 r_{ij,\alpha} r_{ij,\beta} - \frac{1}{2}f_1(r_{ij,\alpha}d_{i,\beta} + r_{ij,\beta}d_{i,\alpha})\right] \tag{24}$$

where $\mathbf{d}_i^I = \mathbf{r}_i^I - \mathbf{r}^I$ is the distance vector between site i and the center of mass of rigid unit I. The last term in eq 24 can be seen as a correction term for keeping the unit rigid.

The Ewald summation is the best way yet devised to accurately compute the long-range interactions between charges in nanoporous materials.[74] It was developed by Ewald to study ionic crystals.[75] The Ewald scheme computes the interactions with all other particles in the simulation cell and with all of their images in an infinitely large array of periodic cells (see the Supporting Information and refs 76−79 for more details). We assume tinfoil boundary conditions (omitting the surface term) and present only the results for the Fourier term. The real part of the Ewald and the exclusion term (to subtract pairs of charges to be excluded for the charge−charge interaction) follow the pair potential formalism. The analogues for f, f_1, and f_2 for the Fourier part of the Ewald summation are

$$f = \frac{1}{k^2} e^{-k^2/4\kappa^2} \{ [\sum_{L,l\in L} q_l^L \cos(\mathbf{k}\cdot\mathbf{r}_l^L)]^2 + [\sum_{L,l\in L} q_l^L \sin(\mathbf{k}\cdot\mathbf{r}_l^L)]^2 \} \tag{25}$$

$$f_1(I) = \frac{2}{k^2} e^{-k^2/4\kappa^2} \{ -[\sum_{L,l\in L} q_l^L \cos(\mathbf{k}\cdot\mathbf{r}_l^L)] q_i^I \sin(\mathbf{k}\cdot\mathbf{r}_i^I) + [\sum_{L,l\in L} q_l^L \sin(\mathbf{k}\cdot\mathbf{r}_l^L)] q_i^I \cos(\mathbf{k}\cdot\mathbf{r}_i^I) \} \tag{26}$$

$$f_2(I) = \frac{2}{k^2} e^{-k^2/4\kappa^2} \{ -[\sum_{L,l\in L} q_l^L \cos(\mathbf{k}\cdot\mathbf{r}_l^L)] q_i^I \cos(\mathbf{k}\cdot\mathbf{r}_i^I) - [\sum_{L,l\in L} q_l^L \sin(\mathbf{k}\cdot\mathbf{r}_l^L)] q_i^I \sin(\mathbf{k}\cdot\mathbf{r}_i^I) \} \tag{27}$$

$$f_2(I,J) = \frac{2}{k^2} e^{-k^2/4\kappa^2} \{ -q_i^I \cos(\mathbf{k}\cdot\mathbf{r}_i^I) q_j^J \cos(\mathbf{k}\cdot\mathbf{r}_j^J) - q_i^I \sin(\mathbf{k}\cdot\mathbf{r}_i^I) q_j^J \sin(\mathbf{k}\cdot\mathbf{r}_j^J) \} \tag{28}$$

where q_i^I is the charge of site i of rigid unit I, $k = |\mathbf{k}|$, and κ is the screening parameter. Note that properties based on f_2 require a double summation over rigid units.

The summation over wavevectors can then be written as

$$U = \frac{1}{4\pi\varepsilon_0} \frac{2\pi}{V} \sum_{\mathbf{k}\neq 0} f = \frac{1}{2V\varepsilon_0} \sum_{\mathbf{k}\neq 0} f \tag{29}$$

where ε_0 is the dielectric constant of vacuum.

The first derivatives with respect to position and orientation are given by

$$\frac{\partial U}{\partial r_{i,\alpha}^I} = \frac{1}{2V\varepsilon_0} \sum_{\mathbf{k}\neq 0} f_1(I) k_\alpha \tag{30}$$

$$\frac{\partial U}{\partial p_{i,\alpha}^I} = \frac{1}{2V\varepsilon_0} \sum_{\mathbf{k}\neq 0} f_1(I) (\mathbf{k}\cdot\mathbf{R}_\alpha^I \mathbf{r}_i^0) \tag{31}$$

The strain derivative of the Fourier part of the Ewald summation reads

$$\frac{\partial U}{\partial \eta_{\alpha\beta}} = \frac{1}{2V\varepsilon_0} \sum_{\mathbf{k}\neq 0} \left[-f\Theta_{\alpha\beta} - f_1(I) \frac{1}{2} (d_\alpha^I k_\beta + d_\beta^I k_\alpha) \right] \tag{32}$$

where

$$\Theta_{\alpha\beta} = \delta_{\alpha\beta} - 2\frac{k_\alpha k_\beta}{\lambda^2} \tag{33}$$

$$\frac{1}{\lambda^2} = \frac{1}{4\alpha^2} + \frac{1}{k^2} \tag{34}$$

Here, $\delta_{\alpha\beta}$ is the Kronecker delta, equal to 1 if $\alpha = \beta$ and 0 otherwise. The second derivatives for pairwise interactions between all of the sites of the rigid units are given in ref 59. Second derivatives of angle-dependent potentials (bend and dihedral) are tedious to derive and implement but are given in the freely available source of the Dynamo code[70] and also refs 80 and 81.

The Fourier expressions for center of mass and orientational second derivatives read

$$\frac{\partial^2 U}{\partial r_\alpha^I \partial r_\beta^J} = \frac{1}{2V\varepsilon_0} \sum_{\mathbf{k}\neq 0} k_\alpha k_\beta [\delta_{IJ} f_2(I) - f_2(I,J)] \tag{35}$$

$$\frac{\partial^2 U}{\partial r_\alpha^I \partial p_\beta^J} = \frac{1}{2V\varepsilon_0} \sum_{\mathbf{k}\neq 0} k_\alpha [\delta_{IJ} f_2(I) (\mathbf{k}\cdot\mathbf{R}_\beta^I \mathbf{r}_i^0) - f_2(I,J) (\mathbf{k}\cdot\mathbf{R}_\beta^J \mathbf{r}_j^0)] \tag{36}$$

$$\frac{\partial^2 U}{\partial p_\alpha^I \partial p_\beta^J} = \frac{1}{2V\varepsilon_0} \sum_{\mathbf{k}\neq 0} \{ \delta_{IJ} [f_2(I) (\mathbf{k}\cdot\mathbf{R}_\alpha^I \mathbf{r}_i^0)(\mathbf{k}\cdot\mathbf{R}_\beta^I \mathbf{r}_i^0) + f_1(I) (\mathbf{k}\cdot\mathbf{R}_{\alpha\beta}^I \mathbf{r}_i^0)] - f_2(I,J) (\mathbf{k}\cdot\mathbf{R}_\alpha^I \mathbf{r}_i^0)(\mathbf{k}\cdot\mathbf{R}_\beta^J \mathbf{r}_j^0) \} \tag{37}$$

The atomic expression for the Hessian can be written out explicitly as

$$\frac{\partial^2 U}{\partial r_{i\alpha} \partial r_{j\beta}} = \frac{1}{V\varepsilon_0} \sum_{\mathbf{k}\neq 0} \frac{e^{-k^2/4\kappa^2}}{k^2} k_\alpha k_\beta \{ -\delta_{ij} [(\sum_{l=1}^N q_l \cos(\mathbf{k}\cdot\mathbf{r}_l)) q_j \cos(\mathbf{k}\cdot\mathbf{r}_j) + (\sum_{l=1}^N q_l \sin(\mathbf{k}\cdot\mathbf{r}_l)) q_j \sin(\mathbf{k}\cdot\mathbf{r}_j)] + [q_i \cos(\mathbf{k}\cdot\mathbf{r}_i) q_j \cos(\mathbf{k}\cdot\mathbf{r}_j) + q_i \sin(\mathbf{k}\cdot\mathbf{r}_i) q_j \sin(\mathbf{k}\cdot\mathbf{r}_j)] \} \tag{38}$$

and is similar to the expression given by Krishnan and Balasubramanian.[80] Note that the Hessian requires a double summation over particles.

The derivatives of the energy with respect to strain and center of mass position and of the energy with respect to strain and orientation for pair potentials are given by

$$\frac{\partial U}{\partial \eta_{\alpha\beta} \partial r_\gamma^I} = f_2 r_{ij,\alpha} r_{ij,\beta} r_{ij,\gamma} + f_1 (\delta_{\alpha\gamma} r_{ij,\beta} + \delta_{\beta\gamma} r_{ij,\alpha}) + \frac{1}{2} [d_\beta^{II} (f_2 r_{ij,\gamma} r_{ij,\alpha} + f_1 \delta_{\alpha\gamma}) + d_\alpha^{II} (f_2 r_{ij,\gamma} r_{ij,\beta} + f_1 \delta_{\beta\gamma})] \tag{39}$$

$$\frac{\partial U}{\partial \eta_{\alpha\beta}\partial p^I_\gamma} = \frac{1}{2}[r_{ij,\beta} + d^{JI}_\beta][f_2(\mathbf{r}_{ij}\cdot\mathbf{R}^I_\gamma\mathbf{r}^0_i)r_{ij,\alpha} + f_1(\mathbf{R}^I_\gamma\mathbf{r}^0_i)_\alpha] + \frac{1}{2}[r_{ij,\alpha} + d^{JI}_\alpha][f_2(\mathbf{r}_{ij}\cdot\mathbf{R}^I_\gamma\mathbf{r}^0_i)r_{ij,\beta} + f_1(\mathbf{R}^I_\gamma\mathbf{r}^0_i)_\beta] \quad (40)$$

where $d^{JI}_\alpha = (d^J_{j,\alpha} - d^I_{i,\alpha})$.

The Fourier expressions for center of mass and orientational cross derivatives read

$$\frac{\partial^2 U}{\partial \eta_{\alpha\beta}\partial r^I_\gamma} = \frac{1}{2V\varepsilon_0}\sum_{\mathbf{k}\neq 0}\Big\{-\delta_{IJ}f_1(I)\Theta_{\alpha\beta}k_\gamma - \delta_{IJ}\frac{1}{2}f_2(I)[d^I_{i,\alpha}k_\beta + d^I_{i,\beta}k_\alpha]k_\gamma + \frac{1}{2}f_2(I,J)[d^J_{j,\alpha}k_\beta + d^J_{j,\beta}k_\alpha]k_\gamma\Big\} \quad (41)$$

$$\begin{aligned}\frac{\partial^2 U}{\partial \eta_{\alpha\beta}\partial p^I_\gamma} = \frac{1}{2V\varepsilon_0}\sum_{\mathbf{k}\neq 0}\{&-\delta_{IJ}f_1(I)\Theta_{\alpha\beta}(\mathbf{k}\cdot\mathbf{R}^I_\gamma\mathbf{r}^0_i) - \\ &\delta_{IJ}\frac{1}{2}f_2(I)(\mathbf{k}\cdot\mathbf{R}^I_\gamma\mathbf{r}^0_i)[d^I_{i,\alpha}k_\beta + d^I_{i,\beta}k_\alpha] \\ -\delta_{IJ}f_1(I)&\frac{1}{2}[(\mathbf{R}^I_\gamma\mathbf{r}^0_i)_\alpha k_\beta + (\mathbf{R}^I_\gamma\mathbf{r}^0_i)_\beta k_\alpha] + \\ &\frac{1}{2}f_2(I,J)(\mathbf{k}\cdot\mathbf{R}^I_\gamma\mathbf{r}^0_i)[d^J_{j,\alpha}k_\beta + d^J_{j,\beta}k_\alpha]\}\end{aligned} \quad (42)$$

For pair potentials we find the strain−strain derivative is given by

$$\begin{aligned}\frac{\partial U}{\partial \eta_{\alpha\beta}\partial \eta_{\mu\nu}} = &\\ &\frac{1}{2}f_2[(r_{ij,\alpha} + d^{JI}_\alpha)r_{ij,\beta}r_{ij,\mu}r_{ij,\nu} + r_{ij,\alpha}(r_{ij,\beta} + d^{JI}_\beta)r_{ij,\mu}r_{ij,\nu}] \\ &+\frac{1}{2}f_1[\delta_{\beta\nu}(r_{ij,\alpha} + d^{JI}_\alpha)r_{ij,\mu} + \delta_{\alpha\nu}(r_{ij,\beta} + d^{JI}_\beta)r_{ij,\mu} + \\ &\quad\delta_{\beta\mu}(r_{ij,\alpha} + d^{JI}_\alpha)r_{ij,\nu} + \delta_{\alpha\mu}(r_{ij,\beta} + d^{JI}_\beta)r_{ij,\nu}] \\ &\quad+\frac{1}{4}f_2[((r_{ij,\alpha} + d^{JI}_\alpha)r_{ij,\beta} + \\ &\quad(r_{ij,\beta} + d^{JI}_\beta)r_{ij,\alpha})(d^{JI}_\mu r_{ij,\nu} + d^{JI}_\nu r_{ij,\mu})] \\ &+\frac{1}{4}f_1[\delta_{\beta\nu}(r_{ij,\alpha} + d^{JI}_\alpha)d^{JI}_\mu + \delta_{\alpha\nu}(r_{ij,\beta} + d^{JI}_\beta)d^{JI}_\mu + \\ &\quad\delta_{\beta\mu}(r_{ij,\alpha} + d^{JI}_\alpha)d^{JI}_\nu + \delta_{\alpha\mu}(r_{ij,\beta} + d^{JI}_\beta)d^{JI}_\nu]\end{aligned} \quad (43)$$

The first two terms in eq 43 correspond to the strain derivative of the first term in eq 24, while the last two terms in eq 43 arise from the second term in eq 24. For atomic systems, eq 43 reduces to the familiar expression derived by Ray[54,82]

$$\frac{\partial U}{\partial \eta_{\alpha\beta}\partial \eta_{\mu\nu}} = f_2 r_{ij,\alpha}r_{ij,\beta}r_{ij,\mu}r_{ij,\nu} + \frac{1}{2}f_1[\delta_{\beta\nu}r_{ij,\alpha}r_{ij,\mu} + \delta_{\alpha\nu}r_{ij,\beta}r_{ij,\mu} + \delta_{\beta\mu}r_{ij,\alpha}r_{ij,\nu} + \delta_{\alpha\mu}r_{ij,\beta}r_{ij,\nu}] \quad (44)$$

The strain−strain derivative for the Fourier part of the Ewald summation is given by

$$\begin{aligned}\frac{\partial U}{\partial \eta_{\alpha\beta}\partial \eta_{\mu\nu}} = &\\ &\frac{1}{2V\varepsilon_0}\sum_{\mathbf{k}\neq 0}\Big\{f\Omega_{\alpha\beta\mu\nu} + \frac{1}{2}f_1(I)[\Theta_{\mu\nu}(d^I_{i,\alpha}k_\beta + d^I_{i,\beta}k_\alpha) + \\ &\quad\Theta_{\alpha\beta}(d^I_{i,\mu}k_\nu + d^I_{i,\nu}k_\mu)] \\ &+\frac{1}{4}f_2(I)(d^I_{i,\alpha}k_\beta + d^I_{i,\beta}k_\alpha)(d^I_{i,\mu}k_\nu + d^I_{i,\nu}k_\mu) - \\ &\quad\frac{1}{4}f_2(I,J)[d^I_{i,\alpha}k_\beta + d^I_{i,\beta}k_\alpha][d^J_{j,\mu}k_\nu + d^J_{j,\nu}k_\mu] \\ &+\frac{1}{4}f_1(I)[\delta_{\beta\nu}(k_\alpha d^I_{i,\mu}) + \delta_{\alpha\nu}(k_\beta d^I_{i,\mu}) + \\ &\quad\delta_{\beta\mu}(k_\alpha d^I_{i,\nu}) + \delta_{\alpha\mu}(k_\beta d^I_{i,\nu})]\end{aligned} \quad (45)$$

where

$$\begin{aligned}\Omega_{\alpha\beta\mu\nu} = &\ \Theta_{\alpha\beta}\Theta_{\mu\nu} + (\delta_{\alpha\mu}\delta_{\beta\nu} + \delta_{\alpha\nu}\delta_{\beta\mu}) + 4\frac{k_\alpha k_\beta k_\mu k_\nu}{k^4} \\ &- 2\frac{k_\alpha k_\nu\delta_{\beta\mu} + k_\beta k_\nu\delta_{\alpha\mu} + k_\beta k_\mu\delta_{\alpha\nu} + k_\alpha k_\mu\delta_{\beta\nu}}{\lambda^2} \\ &- \frac{1}{2}(\Theta_{\alpha\nu}\delta_{\beta\mu} + \Theta_{\beta\nu}\delta_{\alpha\mu} + \Theta_{\beta\mu}\delta_{\alpha\nu} + \Theta_{\alpha\mu}\delta_{\beta\nu})\end{aligned} \quad (46)$$

The expression for the Ewald summation reduces for atoms to the equation given by Van Workum et al.[83]

$$\frac{\partial U}{\partial \eta_{\alpha\beta}\partial \eta_{\mu\nu}} = \frac{1}{2V\varepsilon_0}\sum_{\mathbf{k}\neq 0} f\Omega_{\alpha\beta\mu\nu} \quad (47)$$

Strain-strain derivatives for the angle dependent potentials, e.g., bend and torsion potentials, are derived by Van Workum et al.[84] Cross potentials, e.g., bend-torsion coupling, are easily handled using the chain rule. More details on angle derivatives and elimination of singularities are given in refs 85−87.

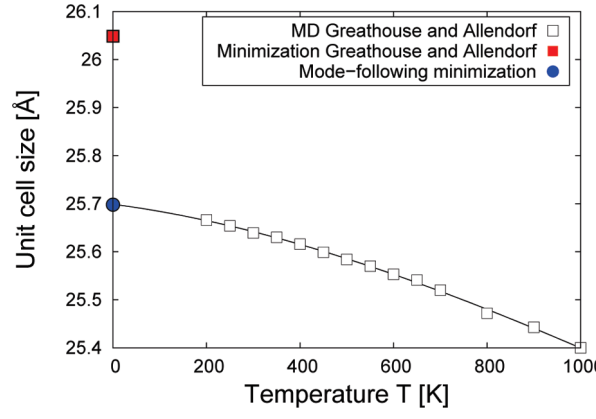

Figure 2. Size of the unit cell of IRMOF-1 predicted by the model of Greathouse and Allendorf.[27] MD data are taken from their work. Their work predicts that the minimized structure is 26.0484 Å. However, when we fit a spline through their 200−1000 K MD data, the extrapolated value is 25.698 Å at 0 K. We find the inconsistent value of 26.0484 Å is the value predicted by methods like conjugate gradient and Newton−Raphson, while the correct value of 25.698 Å is given by the mode-following minimization.

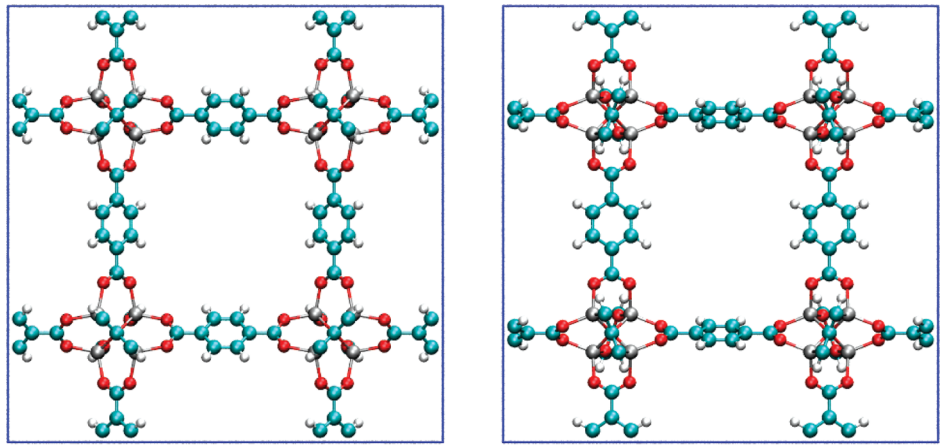

Figure 3. IRMOF-1 structure at 0 K using the model of (a) this work and (b) Greathouse and Allendorf. The model presented in this work predicts a unit cell edge length of 25.965 Å and space group $Fm\bar{3}m$ (225), while the model of Greathouse and Allendorf predicts a unit cell edge length of 25.698 Å and space group $Fm\bar{3}m$ (202). Note the distortion of the metal nodes in panel b. The minimization method for both models was a mode-following technique that guarantees all eigenvalues of the Hessian are positive. A space group of P1 was used. Oxygens are shown in red, zinc in silver, carbon in cyan, and hydrogen in white.

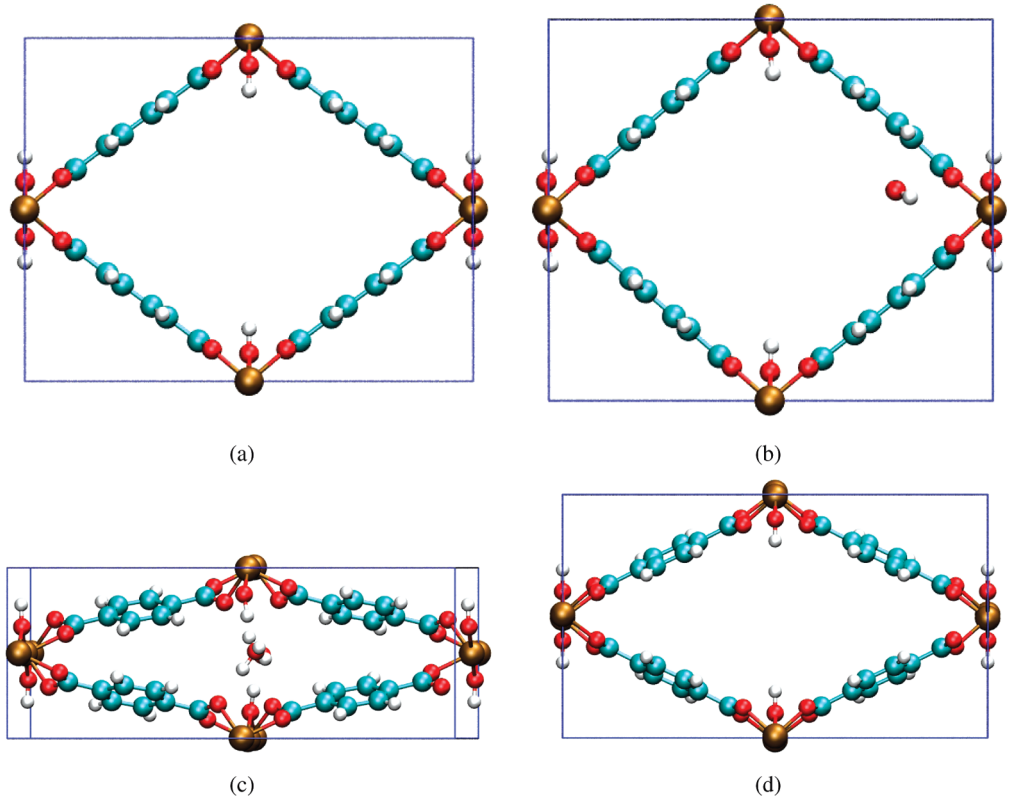

Figure 4. Minimization of MIL-53 systems at different water loadings: (a) no water, (b) one water molecule per unit cell, (c) two water molecules per unit cell, and (d) a saddle point obtained by starting from (a) following the softest mode of the system. Here, for this transition state all gradients are zero but there is a single negative eigenvalue. The method for (a), (b), and (c) was the mode-following minimization technique that guarantees all eigenvalues of the generalized Hessian are positive. A space group of P1 was used. The viewpoint of all four panels is the same. The β angle for panels a, b, and d is 90°, while for panel c, the β angle is 98.683°. Oxygens are shown in red, chromium in ochre, carbon in cyan, and hydrogen in white.

Case Study 1: Determination of the Structure of IRMOF-1 at 0 K

The first case study will show that mode-following minimization is sometimes vital to ensure that the correct structure is obtained at 0 K. The specific example we study here is one of the IRMOF compounds developed by Yaghi and co-workers.[4−6,8,88] In general, IRMOFs consist of zinc−oxygen complexes connected by carboxylate-terminated linkers, forming a regular, three-dimensional lattice of cubic cavities. The linker molecules are, for example, 1,4-benzenedicarboxylate for IRMOF-1 and biphenyldicarboxylate for IRMOF-10. In IRMOF-1, the linkage of the zinc−oxygen complexes alternates between linkers pointing outward and inward. This results in a structure that contains two alternating cavities of about 14.3 and 10.9 Å in diameter. The structure of IRMOF-1 is known from crystallography: edge lengths are

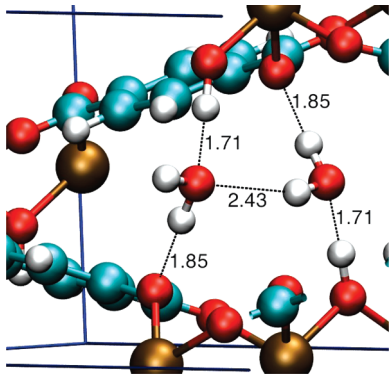

Figure 5. Hydrogen bond distances between water−water and water−host MIL-53 using the model of Salles et al.[34]

25.8849 Å at 213 K and the space group is $Fm\bar{3}m$ (225).[4] This prototypical IRMOF is difficult to minimize because of the many soft modes in the system.

The model of Greathouse and Allendorf[26] was one of the first models for IRMOFs. The CVFF model[36] was used for the linker molecules, while the corners were simulated with nonbonded potentials. Using this model, they showed that water attacks the corners and slowly destroys the structure. Later, experimental verification of this theoretical prediction followed.[89] In ref 27, they showed the minimization result for their model, but this result was in discrepancy with their molecular dynamics results (see Figure 2 and Figures 1 and 2 in ref 27). Clearly, the extrapolation of the finite temperature to 0 K does not coincide with the minimized structure given by Greathouse and Allendorf. This contradiction was left unexplained in the paper.

Using their model, we first minimized the structure using conjugate gradient and Newton−Raphson. Both methods give a structure with 26.0484 Å edge lengths and cell angles of 90°. These are also the values reported by Greathouse and Allendorf. However, this structure has 32 negative eigenvalues. When we apply the mode-following minimization, which slowly eliminates the negative eigenvalues, we obtain a structure having edge lengths of 25.698 Å, in agreement with the extrapolated MD result. A movie that tracks the optimization process starting from the experimental structure[5] is provided as Supporting Information. This structure is the true minimum for this model. However, upon examination, one notices that the Zn_4O units are distorted and asymmetric, in disagreement with the experimental structure (Figure 3b). (Note that the experimental structure is obtained at higher temperature, but it seems reasonable that the symmetry of the Zn_4O units should be maintained.) In addition, the linkers have rotated, and the space group has changed from $Fm\bar{3}m$ (225) to $Fm\bar{3}$ (202). For this model, the value for the bulk modulus at 0 K is 8.77 GPa, and Young's modules is 22.96 GPa. These values do not agree well with published DFT results of a bulk modulus of 16.3 GPa and Young's modulus of 21.9 GPa (see ref 27 and references therein).

In ref 28, we developed a similar model but calibrated the parameters to reproduce the experimental unit cell size and adsorption properties. Using this model, we previously predicted that the IRMOFs possess negative thermal expansion coefficients (a counterintuitive property that the structure contracts when heated and expands when cooled). We recently developed and used a refined model[90] showing that the influence of framework flexibility on diffusion of alkanes and benzene in IRMOF-1 is

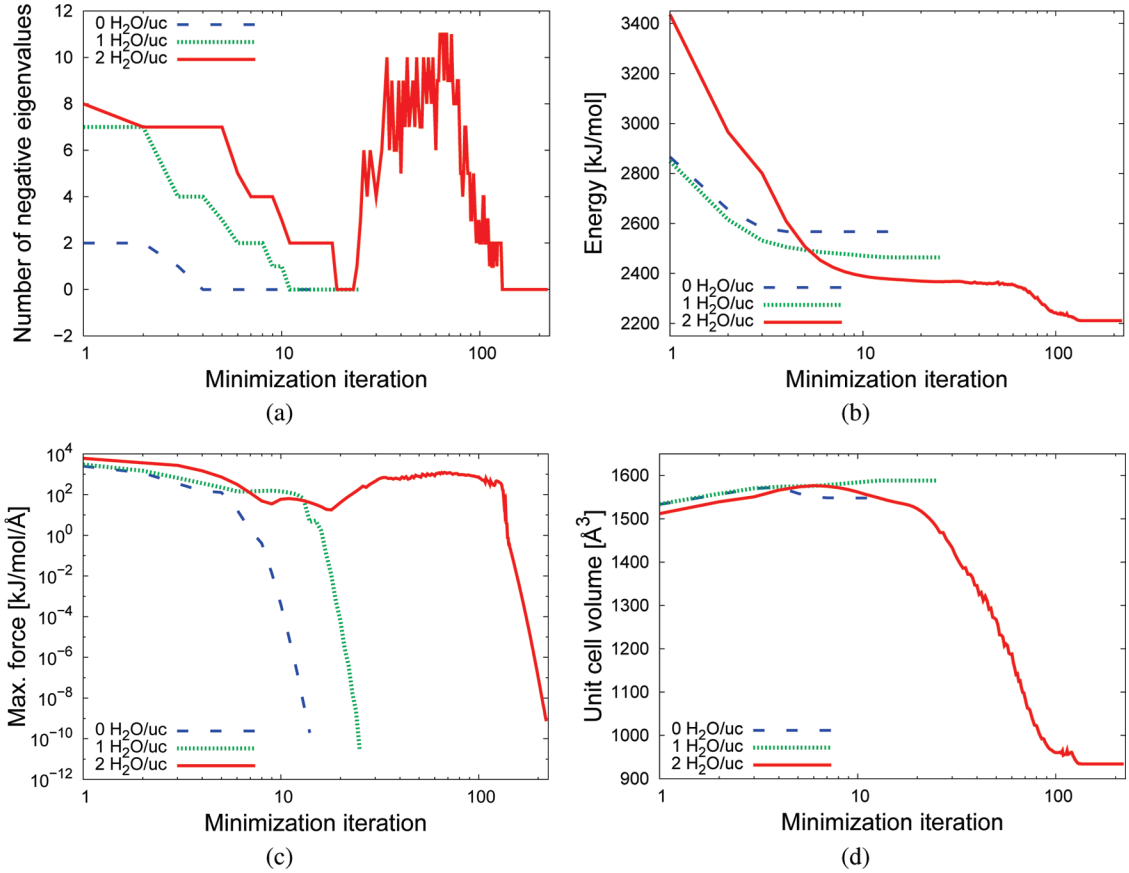

Figure 6. Mode-following minimization of MIL-53 using the model of Salles et al.[34] with zero, one, and two water molecules per unit cell: (a) number of negative eigenvalues, (b) convergence of energy, (c) convergence of maximum of the gradients on the particles (translation and rotational) and cell, and (d) volume of unit cell.

rather small. The changes in the model reflect a better representation of the carboxylate group and are described in the Supporting Information. Again for this model, we used the mode-following minimization method to find the minimum energy structure starting from the experimental structure.[88] The minimum is found in only six iterations, and for this model, the Zn_4O units retain their symmetry as shown in Figure 3a. Because of the temperature difference (the experimental structure is for 258 K), the structure expands somewhat in size but hardly in fractional positions (Supporting Information). For our model, the predicted bulk modulus is 17.7 GPa and Young's modulus is 22.42 GPa, both of which are in excellent agreement with the DFT values (16.3 and 21.9 GPa, respectively).

At the minimum energy configuration, we can analyze the system by calculating the spectra (from the eigenvalues) and normal modes (from the eigenmodes). The Hessian is mass-weighted, the eigenvalues and eigenmodes are computed, and the eigenmodes are unweighted afterward.[70] In the Supporting Information, we include a movie of the softest eigenmode of the IRMOF-1 system with 10 water molecules adsorbed. Eigenmodes are very helpful for providing insight into the movement of the framework. Given the normal modes and frequencies, one can compute dynamic and thermodynamic properties. Normal mode calculations can be compared directly with vibrational spectra, and the method is often used to adjust potential energy function force constants.

Case Study 2: Influence of Water on the Structure of MIL-53

Extreme examples of framework flexibility are the "breathing MOFs", with the MIL-53 structure as a prime example.[11] Pore breathing structures can expand or shrink to admit guest molecules. MIL-53 is a three-dimensional MOF containing unidirectional diamond-shaped channels. The open form of MIL-53 (MIL-53lp) is obtained upon calcination of the as-synthesized compound, while the adsorption of water at room temperature leads to the closed, narrow-pore form (MIL-53np). Upon heating, water adsorption is reversed, leading to a recovery of the open form.[11,12] The difference between the open and closed form is striking. Although the bonded topology is unchanged, some atomic positions change by more than 5 Å, and the unit cell volume decreases by 30% upon going from the open to the closed form.[35]

We used the model of Salles et al.[34] with small modifications (in the original model the C−H and hydroxyl distance was kept fixed). For the water model, we used TIP5P-EW,[62] a modified version of the TIP5P model suitable for the Ewald summation. The cutoff for the Lennard-Jones potential was 12 Å, and the unit cell was surrounded by 3 × 5 × 5 "replica" unit cells.

In Figure 4, the minimized configurations are shown for zero, one, and two water molecules per unit cell. These final configurations were the lowest energy structures over 1000 minimizations with random starting positions for the water molecules. The Supporting Information contains a movie of the minimization process of MIL-53 with two water molecules per unit cell. In agreement with experiments (and other simulations using a different model[35]) the first water molecule only slightly distorts the structure, but the second water molecule leads to a closed form of MIL-53. Data are listed in Table S18 of the Supporting Information.

The structure with two water molecules and the hydrogen bonds between the water and the water−framework are shown

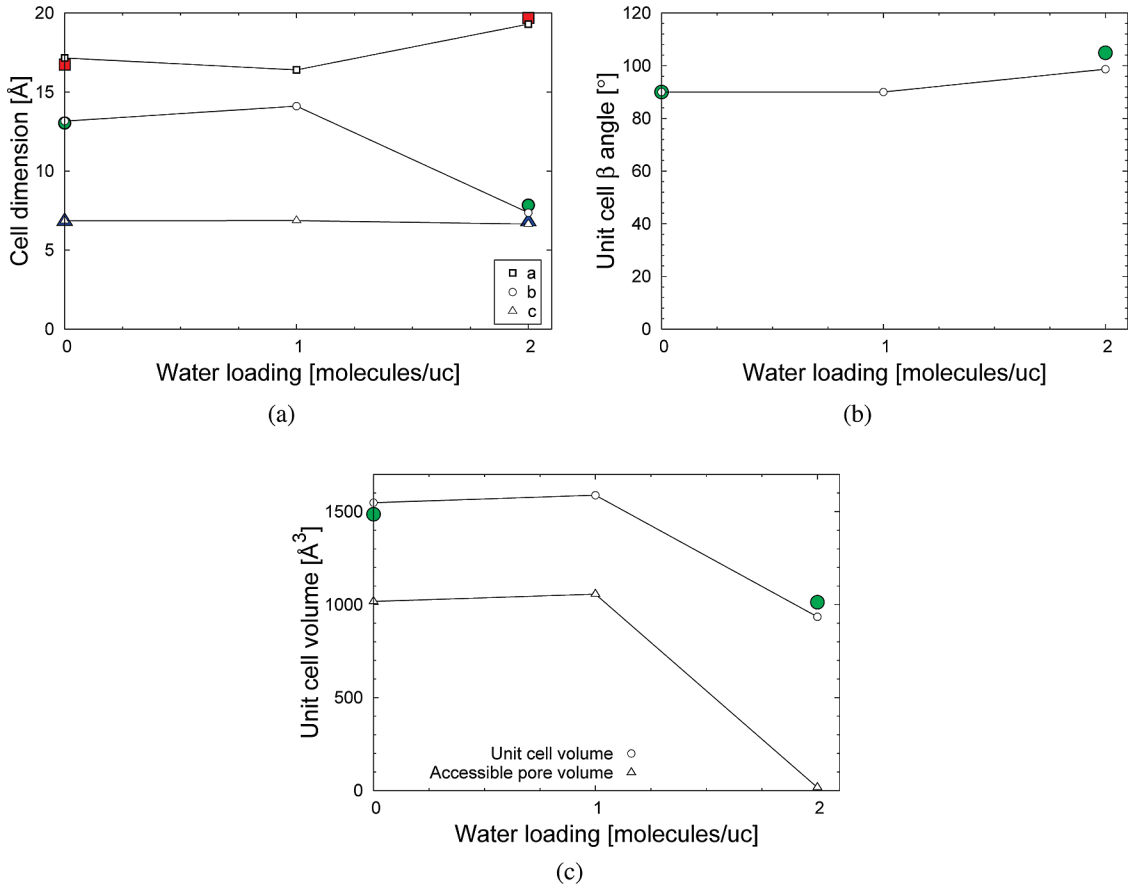

Figure 7. Cell properties of MIL-53 at 0 K: (a) unit cell edge length *a*, *b*, and *c*, (b) β angle, and (c) unit cell volume and simulation values for the accessible pore volume, determined by He probe insertion technique of Talu and Myers.[92] Simulations (open points) used the model of Salles et al.[34] Experimental data (filled symbols) are taken from ref 35.

in Figure 5. The short distances, especially of the water with the framework, and the amount of bonds indicate that the hydrogen bonds are very strong in this system. The distance of the oxygen of the water and the hydrogen of the framework hydroxyl group is 1.71 Å, distance between the hydrogen of the water and the oxygen of the carboxylate group of the framework is 1.85 Å, and distance between the oxygen of the water and the hydrogen of the neighboring water is 2.43 Å. The typical length of a hydrogen bond in water is 1.97 Å.

The minimization process is shown in Figure 6 for the MIL-53 with zero, one, or two water molecules per unit cell. The initial configuration is the experimental crystal structure[91] with the water at random positions. The figures and minimization movie show the result for the lowest energy. Initially, there are many negative eigenvalues present, and the number increases with the amount of water in the system. The number of minimization steps therefore depends on the amount and initial positions of the adsorbates. Slowly but steadily the number of negative eigenvalues is reduced to zero, although it is possible that the number increases before decreasing again. This usually corresponds to a substantial structural change. As can be seen, once zero eigenvalues have been reached, the convergence is very fast. In this work, the stopping criteria has been that all of the gradients on the particles and cell have to be smaller than 10^{-10} kJ/mol/Å. We also kept track of the volume during the minimization. Initially, the gradients are high and volume increases. This behavior increases with water content because the water is placed randomly inside the structure. During the minimization, the structure relaxes, and for zero or one water molecule per unit cell, the volume stays close to the open pore starting structure. However, when two water molecules are optimized, the structure collapsed to the narrow pore structure.

The mode-following method can be used to minimize unit cells, but it can also be used to search for saddle points. In Figure 4d, the result is shown for a saddle point search starting from a minimized MIL-53 without water (Figure 4a) and following the softest mode of the system. These soft modes often correspond to large structural changes. If we compare the data of Table S19 of the Supporting Information with Table S18 of the Supporting Information, then this state can indeed be viewed as one of the intermediate configurations when the MIL-53lp changes to MIL-53np.

The minimization results are more quantitatively plotted in Figure 7. For zero, one, and two water molecules per unit cell of MIL-53, we show the cell dimensions, unit cell β angle, and unit cell volume. The result for zero or one water molecule per unit cell matches very well with the experimentally found open structure MIL-53lp, while the result for two water molecules per unit cell matches well with the experimentally found closed structure MIL-53np. Both the Salles model[34] and model of Coombes[35] seem to capture this effect almost quantitatively.

In order to further underline the significant structural changes on water adsorption, we determined the accessible pore volume using the helium probe insertion simulation technique of Talu and Myers;[92] this data is also plotted in Figure 7c. We note that the structure at two molecules per unit cell of water adsorbed is essentially inaccessible to other guest molecules. In the Figure S4 of the Supporting Information we show that for future simulations of adsorption in MIL-53 it is important to include flexibility. The model of Salles et al. needs to be modified to improve the reproduction of currently available experimental data.

Conclusion

We have presented a powerful method to quickly calculate and analyze the structure of ordered crystalline nanoporous materials at 0 K. The mode-following minimization technique was combined with a matrix formalism for rigid bodies, so that rigid guest molecules are easily treated in a flexible host. The necessary expressions were derived in this paper. The resulting minimization method is fast, stable, and reliably convergent. It is able to provide the correct solution, i.e., the desired number of negative eigenvalues by construction, where other methods can give the wrong solution. We have shown an example for this failure when minimizing the metal−organic framework IRMOF-1. Using mode-following minimization, the gradients on the cell and particles can be lowered arbitrarily close to zero. In the current work, the gradients on each of the particles and cell matrix were lower than 10^{-10} kJ/mol/Å. The method can be of great utility in force field development and to assess the influence of adsorbates on the framework structure. The methodology developed in this paper is applicable also to determine the crystal structure of layered materials.[93,94]

Acknowledgment. This work is supported by a TOP grant from The Netherlands Foundation for Fundamental Research (NWO−CW) awarded to R.K. and the National Science Foundation (CTS-0507013).

Supporting Information Available: Force field data, additional background material, description of the IRMOF-1 and MIL structures, validation of the computer code, and three avi-movies. This material is available free of charge via the Internet at http://pubs.acs.org.

References and Notes

(1) Snurr, R. Q.; Hupp, J. T.; Nguyen, S. T. *A.I.Ch.E. J.* **2004**, *50*, 1090–1095.
(2) Krishna, R. *J. Phys. Chem. B.* **2009**, *113,* DOI:10.1021/jp906879d.
(3) Jacoby, M. *Chem. Eng. News* **2008**, *86*, 13–16.
(4) Li, H.; Eddaoudi, M.; O'Keeffe, M.; Yaghi, O. M. *Nature* **1999**, *402*, 276–279.
(5) Eddaoudi, M.; Kim, J.; Rosi, N.; Vodak, D.; Wachter, J.; O'Keefe, M.; Yaghi, O. M. *Science* **2002**, *295*, 469–472.
(6) Yaghi, O. M.; O'Keeffe, M.; Ockwig, N. W.; Chae, H. K.; Eddaoudi, M.; Kim, J. *Nature* **2003**, *423*, 705–714.
(7) Kitagawa, S.; Kitaura, R.; Noro, S.-I. *Angew. Chem., Int. Ed.* **2004**, *43*, 2334–2375.
(8) Rowsell, J. L. C.; Yaghi, O. M. *Microporous Mesoporous Mater.* **2004**, *73*, 3–14.
(9) Mueller, U.; Schubert, M.; Teich, F.; Puetter, H.; Schierle-Arndt, K.; Pastre, J. *J. Mater. Chem.* **2006**, *16*, 626–636.
(10) Férey, G. *Chem. Soc. Rev.* **2008**, *37*, 191–214.
(11) Serre, C.; Millange, F.; Thouvenot, C.; Nogues, M.; Marsolier, G.; Louer, D.; Férey, G. *J. Am. Chem. Soc.* **2002**, *124*, 13519–13526.
(12) Devautour-Vinot, S.; Maurin, G.; Henn, F.; Serre, C.; Devic, T.; Férey, G. *Chem. Commun.* **2009**, *19*, 2733–2735.
(13) Bradshaw, D.; Claridge, J. B.; Cussen, E. J.; Prior, T. J.; Rosseinsky, M. J. *Acc. Chem. Res.* **2005**, *38*, 273–282.
(14) Fletcher, A. J.; Thomas, K. M.; Rosseinsky, M. J. *J. Solid State Chem.* **2005**, *178*, 2491–2510.
(15) Bureekaew, S.; Shimomura, S.; Kitagawa, S. *Sci. Technol. Adv. Mater.* **2008**, *9*, 1–12.
(16) Hill, J. R.; Freeman, C. M.; Subramanian, L. *Rev. Comput. Chem.* **2000**, *16*, 141–216.
(17) Demontis, P.; Suffritti, G. B.; Quartieri, S.; Fois, E. S.; Gamba, A. *J. Phys. Chem.* **1988**, *92*, 867–871.
(18) Nicholas, J. B.; Hopfinger, A. J.; Trouw, F. R.; Iton, L. E. *J. Am. Chem. Soc.* **1991**, *113*, 4792–4800.
(19) Hill, J. R.; Sauer, J. *J. Phys. Chem.* **1994**, *98*, 1238–1244.
(20) Hill, J. R.; Sauer, J. *J. Phys. Chem.* **1995**, *99*, 9536–9550.
(21) Dick, B. G.; Overhauser, A. W. *Phys. Rev.* **1958**, *112*, 90–103.
(22) Catlow, C. R. A.; Cormack, A. N.; Theobald, F. *Acta Cryst. B* **1984**, *40*, 195–200.
(23) Schröder, K.-P.; Sauer, J. *J. Phys. Chem.* **1996**, *110*, 11043–11049.
(24) Gale, J. D. *J. Chem. Soc. Faraday Trans.* **1997**, *93*, 629–637.

(25) Gale, J. D.; Rohl, A. L. *Mol. Simul.* **2003**, *29*, 291–341.
(26) Greathouse, J. A.; Allendorf, M. D. *J. Am. Chem. Soc.* **2006**, *128*, 10678–10679.
(27) Greathouse, J. A.; Allendorf, M. D. *J. Phys. Chem. B.* **2008**, *112*, 5795–5802.
(28) Dubbeldam, D.; Walton, K. S.; Ellis, D. E.; Snurr, R. Q. *Angew. Chem., Int. Ed.* **2007**, *46*, 4496–4499.
(29) Amirjalayer, S.; Tafipolsky, M.; Schmid, R. *Angew. Chem., Int. Ed.* **2007**, *46*, 463–466.
(30) Tafipolsky, M.; Amirjalayer, S.; Schmid, R. *J. Comput. Chem.* **2007**, *28*, 1169–1176.
(31) Amirjalayer, S.; Schmid, R. *J. Phys. Chem. B.* **2008**, *112*, 14980–14987.
(32) Han, S. S.; Goddard, W. A. *J. Phys. Chem.* **2007**, *111*, 15185–15191.
(33) Schmid, R.; Tafipolsky, M. *J. Am. Chem. Soc.* **2008**, *130*, 12600–12601.
(34) Salles, F.; Ghoufi, A.; Maurin, G.; Bell, R. G.; Mellot-Draznieks, C.; Férey, G. *Angew. Chem., Int. Ed.* **2008**, *47*, 8487–8491.
(35) Coombes, D. S.; Cora, F.; Mellot-Draznieks, C.; Bell, R. G. *J. Phys. Chem. B.* **2009**, *113*, 544–552.
(36) Dauber-Osguthorpe, P.; Roberts, V. A.; Osguthorpe, D. J.; Wolff, J.; Genest, M.; Hagler, A. T. *Proteins: Struct., Funct., Genet.* **1988**, *4*, 31–47.
(37) Mayo, S. L.; Olafson, B. D.; Goddard, W. A. *J. Phys. Chem.* **1990**, *94*, 8897–8909.
(38) Rappé, A. K.; Casewit, C. J.; Colwell, K. S.; Goddard, W. A.; Skiff, W. M. J. *J. Am. Chem. Soc.* **1992**, *114*, 10024–10035.
(39) Allinger, N. L.; Yuh, Y. H.; Lii, J.-H. *J. Am. Chem. Soc.* **1989**, *111*, 8551–8566.
(40) Press, W. H.; Flannery, B. P.; Teukolsky, S. A.; Vetterling, W. T. *Numerical Recipes in C*; Cambridge University Press: New York, 1988.
(41) Nelder, J. A. *Comput. J.* **1965**, *7*, 308–313.
(42) Lagarias, J. C.; Reeds, J. A.; Wright, M. H.; Wright, P. E. *SIAM J. Optim.* **1998**, *9*, 112–147.
(43) Snyman, J. A. *Appl. Math. Model.* **1982**, *6*, 449–462.
(44) Snyman, J. A. *Appl. Math. Model.* **1983**, *7*, 216–218.
(45) Banerjee, A.; Adams, N.; Simons, J.; Shepard, R. *J. Phys. Chem.* **1985**, *89*, 52–57.
(46) Baker, J. *J. Comput. Chem.* **1986**, *7*, 385–395.
(47) Pulay, P.; Fogarasi, G. *J. Chem. Phys.* **1992**, *96*, 2856–2860.
(48) Peng, C. Y.; Ayala, P. Y.; Schlegel, H. B.; Frisch, M. J. *J. Comput. Chem.* **1996**, *17*, 49–56.
(49) Baker, J.; Kinghorn, D.; Pulay, P. *J. Chem. Phys.* **1999**, *110*, 4986–4991.
(50) Paizs, B.; Baker, J.; Suhai, S.; Pulay, P. *J. Chem. Phys.* **2000**, *113*, 6566–6572.
(51) Kudin, K. N.; Scuseria, G. E.; Schlegel, H. B. *J. Chem. Phys.* **2001**, *114*, 2919–2923.
(52) Bakken, V.; Helgaker, T. *J. Chem. Phys.* **2002**, *117*, 9160–9174.
(53) Bucko, T.; Hafner, J.; Angyan, J. G. *J. Chem. Phys.* **2005**, *122*, 124508.
(54) Lutsko, J. F. *J. Appl. Phys.* **1989**, *65*, 2991–2997.
(55) Humphrey, W.; Dalke, A.; Schulten, K. *J. Mol. Graph.* **1996**, *14*, 33–38.
(56) Schroeder, W.; Martin, K.; Lorensen, B. *The Visualization Toolkit: An Object-Oriented Approach to 3D Graphics*; Prentice-Hall, Inc: Upper Saddle River, NJ, 1996.
(57) Visualization Toolkit (VTK). http://www.vtk.org.
(58) Willock, D. J.; Price, S. L.; Leslie, M.; Catlow, C. R. A. *J. Comput. Chem.* **1995**, *16*, 628–647.
(59) Chakrabarti, D.; Wales, D. J. *Phys. Chem. Chem. Phys.* **2009**, *11*, 1970–1976.
(60) Jenkins, R.; Snyder, R. L. *Introduction to X-ray Powder Diffractometry*; John Wiley & Sons: New York, 1996.
(61) Pecharsky, V. K.; Zavalij, P. Y. *Fundamentals of Powder Diffraction and Structural Characterization of Materials*; Springer: New York, 2005.
(62) Ricks, S. W. *J. Chem. Phys.* **2004**, *120*, 6085–6093.
(63) Rai, N.; Siepmann, J. I. *J. Phys. Chem. B.* **2007**, *111*, 10790–10799.
(64) Potoff, J. J.; Siepmann, J. I. *A.I.Ch.E. J.* **2001**, *47*, 1676–1682.
(65) Dillen, J. L. M. *J. Comput. Chem.* **1986**, *7*, 476–481.
(66) Dillen, J. L. M. *J. Comput. Chem.* **1987**, *8*, 1099–1103.
(67) Pulay, P. *Modern Electronic Structure Theory*, Plenum: New York, 1977; p 170.
(68) Lu, D.-H.; Zhao, M.; Truhlar, D. G. *J. Comput. Chem.* **1991**, *12*, 376–384.
(69) Lu, D.-H.; Truhlar, D. G. *J. Chem. Phys.* **1993**, *99*, 2723–2738.
(70) Field, M. J. *A Practical Introduction to the Simulation of Molecular Systems*; Cambridge University Press: New York, 1999.
(71) Cerjan, C. J.; Miller, W. H. *J. Chem. Phys.* **1991**, *75*, 2800–2806.
(72) Simons, J.; Jorgensen, P.; Taylor, H.; Ozment, J. *J. Phys. Chem.* **1983**, *87*, 2745–2753.
(73) Alexeev, Y.; Schmidt, M. W.; Windus, T. L.; Gordon, M. S. *J. Comput. Chem.* **2007**, *28*, 1685–1694.
(74) Vlugt, T. J. H.; Garcia-Perez, E.; Dubbeldam, D.; Ban, S.; Calero, S. *J. Chem. Theory Comp.* **2008**, *4*, 1107–1118.
(75) Ewald, P. P. *Ann. Phys.* **1921**, *369*, 253–287.
(76) Allen, M. P.; Tildesley, D. J. *Computer Simulation of Liquids*; Clarendon Press: Oxford, 1987.
(77) Toukmaji, A. Y.; Board, J. A. *Comput. Phys. Commun.* **1996**, *95*, 73–92.
(78) Nymand, T. M.; Linse, P. *J. Chem. Phys.* **2000**, *112*, 6152–6160.
(79) Aguado, A.; Madden, P. A. *J. Chem. Phys.* **2003**, *119*, 7471–7483.
(80) Krishnan, M.; Balasubramanian, S. *Phys. Rev. B* **2003**, 68; Article number 064304.
(81) Lavor, C. *Physica D* **2007**, *227*, 135–141.
(82) Ray, J. R. *Comput. Phys. Rep.* **1988**, *8*, 111–151.
(83) van Workum, K.; Yoshimoto, K.; de Pablo, J. J.; Douglas, J. F. *Phys. Rev. E* **2005**, 71; Article number 061102.
(84) van Workum, K.; Gao, G.; Schall, J. D.; Harrison, J. A. *J. Chem. Phys.* **2006**, *125*, 144506.
(85) Blondel, A.; Karplus, M. *J. Comput. Chem.* **1996**, *17*, 1132–1141.
(86) Lee, S.-H.; Palmo, K.; Krimm, S. *J. Comput. Chem.* **1999**, *20*, 1067–1084.
(87) Tuzun, R. E.; Noid, D. W.; Sumpter, B. G. *J. Comput. Chem.* **2000**, *21*, 553–561.
(88) Eddaoudi, M.; Moler, D. B.; Li, H.; Chen, B.; Reineke, T. M.; O'Keeffe, M.; Yaghi, O. M. *Acc. Chem. Res.* **2001**, *34*, 319–330.
(89) Kaye, S. S.; Dailly, A.; Yaghi, O. M.; Long, J. R. *J. Am. Chem. Soc.* **2007**, *129*, 14176–14177.
(90) Ford, D. C.; Dubbeldam, D.; Snurr, R. Q. In *Diffusion Fundamentals III*; Chmelik, C., Kanellopoulos, N., Kärger, J., Theodorou, D., Eds.; Leipziger Universitätsverlag: Leipzig, Germany, 2009; pp. 459−466.
(91) Liu, Y.; Her, J.-H.; Dailly, A.; Ramirez-Cuesta, A. J.; Neumann, D. A.; Brown, C. M. *J. Am. Chem. Soc.* **2008**, *130*, 11813–11818.
(92) Talu, O.; Myers, A. L. *A.I.Ch.E. J.* **2001**, *47*, 1160–1168.
(93) Cygan, R. T.; Greathouse, J. A.; Heinz, H.; Kalinichev, A. G. *J. Mater. Chem.* **2009**, *19*, 2470–2481.
(94) Kanoh, H.; Kondo, A.; Noguchi, H.; Kajiro, H.; Tohdoh, A.; Hattori, Y.; Xu, W.-C.; Inoue, M.; Sugiura, T.; Morita, K.; Tanaka, H.; Ohba, T.; Kaneko, K. *J. Colloid Interface Sci.* **2009**, *334*, 1–7.

JP906635F